2026 IEEE International Conference on Robotics and Automation (ICRA 2026)
June 1-5, 2026. Vienna, Austria

Tuning hydrodynamic coefficients using a genetic algorithm for a numerical model of a bio-robotic sea lion*

Shraman Kadapa, Nicholas Marcouiller, Anthony Drago, James L. Tangorra, Harry G. Kwatny

Abstract— **Bio-inspired swimming vehicles are increasingly being developed to understand the locomotion strategies of aquatic animals to expand the performance envelope of engineered systems. However, the increasing complexity of these multi-segmented vehicles makes it challenging to understand and optimize their performance. Accurate numerical models of these systems can provide a pathway forward, but it depends critically on reliable estimation of hydrodynamic coefficients. Traditional approaches to estimate these coefficients, such as tow-tank testing can be costly and often impractical. In this work, a numerical model of a bio-robotic sea lion was developed and validated, in which hydrodynamic coefficients critical for estimating fluid forces were first obtained through computational fluid dynamics (CFD) simulations and analytical methods such as strip theory. These coefficients were then refined using a genetic algorithm to improve agreement with experimental trials of the robot. This hybrid framework bridges the gap between simulation and reality, enabling accurate force estimation across different body segments. Validation experiments showed a close alignment between the numerical model and the physical robot's performance in position and orientation during various trials. The validated model could enable large-scale parametric studies to evaluate the effectiveness of different control surfaces, optimize gaits, and explore control strategies without extensive prototyping of the bio-robotic platform. Beyond design and analysis, the model can also provide a high-fidelity environment for the application of reinforcement learning, supporting the development of adaptive controllers and advancing bio-inspired robots toward autonomous operation.**

I. Introduction

Learning the locomotion strategies of aquatic animals offers a pathway to improve the maneuverability of engineered underwater vehicles [1], [2]. Aquatic species achieve propulsion and control through coordinated motion of multiple body segments and control surfaces, like fins or flippers, enabling robust swimming and turning within turbulent flow environments. Engineers seek to adapt these biological strategies to expand the performance envelope of engineered systems [3]. Existing bio-inspired swimming robots, ranging from fish-like robots [4], [5], and sea turtle robots [6], [7], to eel and sea snake like robots [8], [9], [10], demonstrate diverse locomotion strategies for swimming and navigating complex aquatic environments. While significant progress has been made in developing such systems, the increasing use of multiple body segments and control surfaces makes it challenging to isolate and understand their individual contributions to swimming performance.

Numerical modeling provides a framework to predict and analyze the performance of bio-robotic swimmers, but its accuracy depends critically on the hydrodynamic coefficients used to estimate fluid forces on each body segment. These coefficients vary with instantaneous orientation, configuration, and fluid–structure interaction, making them difficult to generalize across multi-body systems. Bio-robotic systems increasingly incorporate shape-changing features that alter the global geometry to better interact with surrounding flow, yet such reconfigurations further shift the underlying coefficients when considered at the whole-body scale. To manage this complexity, the system must be decomposed into smaller components, where local interactions can be modeled more consistently. Computational fluid dynamics (CFD) has been widely applied to estimate drag forces for these geometries[11], yet added-mass terms remain challenging because they require resolving unsteady accelerations and configuration-dependent inertial effects. It is important to account for added mass effects arising from acceleration of the surrounding fluid during body motion, as these reactive forces have been shown to play a fundamental role in classical biofluid dynamic formulations[12]. Experimental approaches, such as tow-tank tests, can yield these coefficients [13], [14], but they are costly, facility-limited, and impractical for large parameter sweeps. As a result, researchers lack generalizable methods to obtain the coefficient sets needed for validating models of complex, shape-changing bio-robotic systems.

The objective of this study is to develop and validate a numerical model of a bio-robotic sea lion, that leverages a hybrid approach to identify the hydrodynamic coefficients. Computational fluid dynamic (CFD) simulations were applied to discrete segments along the body axis, including the head, main body sections, and pelvis section, consistent with a strip-theory decomposition. This segmentation provided distinct drag and added-mass coefficients for each component, which were combined with analytical strip-

*Research supported by the Office of Naval Research (ONR) (Dr. Thomas McKenna, Program Officer, ONR 341) under grant number N00014-24-1-2536.

Shraman Kadapa is with Drexel University, Philadelphia, PA, USA (corresponding author: e-mail: sk3496@drexel.edu).

Nicholas Marcouiller is with Drexel University, Philadelphia, PA, USA (e-mail: nm875@drexel.edu).

Anthony Drago is with Drexel University, Philadelphia, PA, USA (e-mail: ad892@drexel.edu).

James L Tangorra is with Drexel University, Philadelphia, PA, USA (e-mail: jlt66@drexel.edu).

Harry G Kwatny is with Drexel University, Philadelphia, PA, USA (e-mail: hgk22@drexel.edu).

theory estimates to form an initial coefficient set. A genetic algorithm was then employed to refine these values, with the explicit aim of bringing the numerical model into agreement with experiments on the physical robot. In this framework, CFD supplied a physics-based baseline while the optimization procedure reconciled discrepancies between simulation and reality. Model validity was established by comparing simulated trajectories with experimental trials of the robot across multiple swimming trials. The resulting model enabled a dynamic simulation and analysis of six-degree-of-freedom (6-DoF) body motions in water, providing a validated tool for future control design and gait optimization.

While significant progress has been made to estimate hydrodynamic coefficients for conventional propeller-based systems, it is hard to estimate coefficients for more complex bio-inspired underwater robots. Prior work has primarily focused on simplified hull forms. For instance, [15] compared hydrodynamic derivatives of a crate-shaped vehicle obtained via strip theory with flume experiments, reporting good agreement. Similarly, a dynamic model of a torpedo-shaped vehicle was developed in [16], where drag coefficients were derived from CFD simulations and added-mass derivatives from strip theory. Although this approach has shown success for torpedo-like geometries, there is limited evidence demonstrating the accuracy of this approach across different configurations. In [17], both drag and added-mass coefficients for a crate-shaped vehicle were estimated entirely through CFD, while [18] computed theoretical coefficients for individual control surfaces of a torpedo-shaped UUV. Multi-body robotic systems, where body segments themselves act as control surfaces, add additional challenges to calculating these coefficients as the system can be in many different configurations. Additional challenges come when propulsion is created through flapping or multi-degree of freedom control surfaces. A notable gap in the literature is the absence of accurate estimation and validation for hydrodynamic coefficients and validation of the numerical model for such platforms.

The remainder of this paper is organized as follows. Section II describes the development of the numerical model. Section III presents experimental trials comparing different swimming strokes between the model and the physical robotic platform. Section IV provides a discussion of the results and future directions, and Section V concludes with key takeaways.

II. Methods

A numerical model of a bio-robotic sea lion was previously developed in a Simscape multibody system (The MathWorks, Inc., Portola Valley, CA, USA) to simulate, visualize and analyze the full body motion of the robotic system during swimming and maneuvering trials [19], (Fig. 1). The model included the main body, head, pelvis, and paired fore- and hind flippers, with actuated degrees of freedom matching the physical robot. The model also accounted for the additional mass resulting from the system being open and flooded. Hydrodynamic forces, including drag, lift, lateral forces, and added mass effects, were incorporated using coefficients obtained from CFD and strip theory. Equation (1) represents the equations of motion for a rigid body that is completely submerged in water. Details of the model development and initial coefficient estimation are provided in a prior publication [19]. A detailed description of the design and development of the bio-robotic platform can be found in [20]. The dynamics of the fully submerged multi-body system are governed by the following equation.

$$M(q)\dot{p} + C(p,q)p + F(p,q) = Q \quad (1)$$

where q is the vector of generalized coordinates, p is the linear and angular velocities of the generalized coordinates, M(q) is the mass matrix for the entire robot, C (p, q) is the centripetal and Coriolis matrix, F (p, q) is the internal force vector and Q is the externally applied generalized forces.

Hydrodynamic forces, such as drag, lateral, lift, and added mass, were incorporated into the numerical model to simulate the fluid forces the robot would experience during swimming. The main body was decomposed into eight different segments to account for distributed hydrodynamic loading. Drag coefficients were obtained using computational fluid dynamic (CFD) simulations conducted in COMSOL Multiphysics v6.3 (COMSOL, Inc., Boston, MA, USA). To determine the drag coefficient in the surge (x) direction, the full robot geometry was imported into the CFD environment (Fig. 2a). For the lateral (y) and lift (z) directions, each of the eight body segments was analyzed individually in CFD, and the resulting forces were applied at the center of mass of the corresponding segment using (2) (Fig. 2b). In (2), F_D is the drag force, C_D is the drag coefficient, v is the velocity, ρ is the density of water, and A is the area. The fore and hind flippers were modeled as flat plates, and their drag coefficients perpendicular to the incoming flow were assumed to be 1.28. Initial estimates of the added mass coefficients were computed using strip theory formulations. The main body was approximated as a prolate spheroid, and the corresponding added mass coefficients (x: (7), y and z: (8)) were calculated using (3)-(8), where e is the eccentricity of the prolate spheroid, a is the semi-major axis and b is the semi-minor axis, m is the mass and α_0 and β_0 are constants. For the fore flippers and

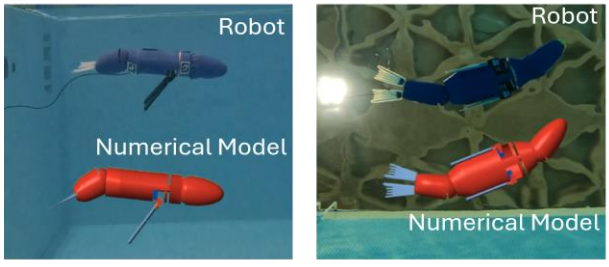

Figure 1. Bio-robotic sea lion and its numerical model during (a) free swimming and (b) maneuvering trials.

hind flippers, the added mass coefficients were computed using (9), where ρ is the density of fluid, k is the coefficient of additional mass [21], b and c denote the span and chord of the rectangular flat plate, respectively.

$$F_D = \frac{1}{2} C_D v^2 \rho A \quad (2)$$

$$e = \sqrt{1-(b/a)^2} \quad (3)$$

$$\alpha_0 = \frac{2(1-e^2)}{e^3}\left(\frac{1}{2} ln \frac{1+e}{1-e} - e\right) \quad (4)$$

$$\beta_0 = \frac{1}{e^2} - \frac{1-e^2}{2e^3} ln \frac{1+e}{1-e} \quad (5)$$

$$m = \frac{4}{3}\pi\rho ab^2 \quad (6)$$

$$X_{\dot{u}} = -\frac{\alpha_0}{2-\alpha_0} m \quad (7)$$

$$Y_{\dot{v}} = Z_{\dot{w}} = -\frac{\beta_0}{2-\beta_0} m \quad (8)$$

$$m_a = \frac{\pi\rho}{4} kbc^2 \quad (9)$$

A genetic algorithm (GA) was implemented in MATLAB (The MathWorks, Inc., Portola Valley, CA, USA) to refine the hydrodynamic coefficients and estimate the volume of water ingress within the robotic system (Fig. 2c). The GA was configured as a multi-objective optimization problem using a Dynamic Time Warping (DTW) function to minimize the error between the simulated and experimental trajectories. The two objectives of the GA were to reduce the position and orientation errors of the robot across two distinct motion profiles: a characteristic sea lion stroke and a characteristic sea lion stroke with pelvis actuation. The dependent variables in the algorithm included: the volume of water inside the robotic system, which directly affects its inertial properties; the coefficients of force in the z-direction, which were refined from initial prolate spheroid estimates to account for the robot's geometry, which is more elongated along the y axis than the z axis; and the offset between the center of mass and center of buoyancy, which was a non-trivial parameter initially estimated by assuming uniform density. The algorithm's parameters were set as follows: a population size of 80, a maximum of 50 generations, and a crossover fraction of 0.8. The multi-objective Pareto front percentage [22] was set to 0.4. Following the optimization runs, the genetic algorithm produced a set of optimal coefficients for each of the two distinct motion profiles. The final coefficients for the numerical model were manually selected from these results by identifying the combination of parameters that provided the best overall fit across both the characteristic stroke and the characteristic stroke with pelvis actuation trials simultaneously. Hydrodynamic coefficients that were optimized by the genetic algorithm are listed in Fig. 2d.

To validate the numerical model, a series of swimming and maneuvering trials were performed experimentally and then replicated in simulation for comparison. The swimming tests examined two distinct strokes: the characteristic stroke and a variation that included pelvis actuation. Both were simulated over three consecutive flipper strokes, with each stroke lasting approximately 2.9 seconds. For maneuvering, pitch and yaw turns were initiated from a forward velocity of 0.31 m/s. During these maneuvers, the head and pelvis sections were actuated simultaneously to 60°. For every experiment, three trials were conducted and averaged. For the numerical model, the same joint actuation profiles used in the experimental platform were prescribed directly at the corresponding revolute joints in simulation. The fore flippers, head, and pelvis were actuated using predefined time-varying angular trajectories, ensuring that the simulated kinematics matched the experimental strokes and maneuvering inputs.

The bio-robotic sea lion was tested in a swimming pool, where video recordings were used to capture its position and

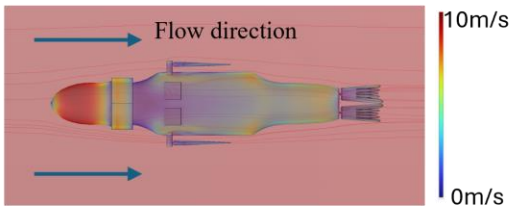

(a)

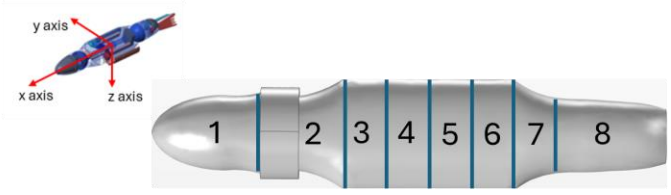

(b)

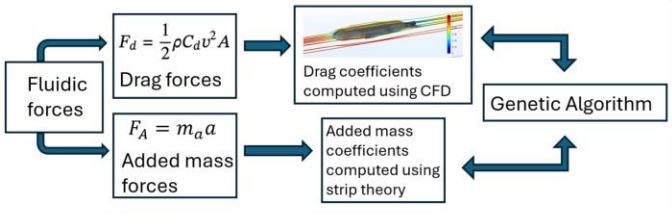

(c)

No.	Parameter	Theoretical	Genetic Algorithm
1	Cd in Z (main body)	0.580	0.754
2	Added mass in Z (main body)	-21.259	-22.996
3	Added mass in X (main body)	-1.171	-1.405
4	Volume of water within robot (%)	100.000	26.000
5	Buoyancy offset for main body(m)	0.010	0.012
6	Buoyancy offset for head (m)	0.000	0.003
7	Buoyancy offset for pelvis (m)	0.000	0.005

(d)

Figure 2. (a) Computational fluid dynamic simulations for the bio-robotic sea lion in x direction. (b) Main body decomposed into eight different segments to compute coefficients of force in y and z directions. (c) General architecture of genetic algorithm. (d) Comparison of coefficients between theoretically computed vs. with genetic algorithm.

orientation during various swimming and maneuvering trials. To ensure a consistent starting pose across trials, the robot was secured to a dock prior to release. The release event was defined as the frame in which the robot was fully disengaged from the dock and free to move. The Video footage was recorded using a GoPro Hero 13 (GoPro, San Mateo, CA, USA), mounted on a perpendicular wall to provide a clear lateral view. The camera captured 4K-resolution footage at 30 frames per second. Two visual markers were placed on the front and rear ends of the robot to facilitate pose tracking. The recorded videos were later analyzed using the image processing toolbox in MATLAB (The MathWorks, Inc., Portola Valley, CA, USA), where the position and orientation of the robot were extracted by tracking the visual markers on the robot. A detailed description of the data collection process is provided in [19].

The numerical model was validated by comparing its center of mass trajectories of both position and orientation against those recorded from the physical robot during trials. For swimming trials, the comparison included metrics such as total distance traveled in surge and heave, the root mean squared error (RMSE) for position and orientation, and the maximum and mean 2D velocity. For maneuvering trials, the analysis focused on the final orientation and mean angular position when head and pelvis were actuated simultaneously during pitch and yaw turns.

In the numerical model, the position and orientation of the robot was sensed at the 6 degrees of freedom joint located on the main body. An ODE 3 (Bogacki-Shampine) solver was used with a fixed time step of 0.001 to solve the equations of motion. Each simulation trial was run for the same duration as the corresponding experimental trial, and initial conditions such as forward velocity and body orientation were matched to those measured at the start of experiments (release event) to ensure consistency. Position and orientation data were also presented with a ±2% buoyancy offset, shown as a red-shaded region, to illustrate the influence of buoyancy variations during each stroke.

III. RESULTS

A. Characteristic Stroke

The numerical model's translational motion during the characteristic stroke closely matched the experimental data in both surge and heave (Fig. 3a). In the surge direction, the robotic system traveled 1.79 m, whereas the numerical model traveled 1.74 m—a difference of only 2.8%.

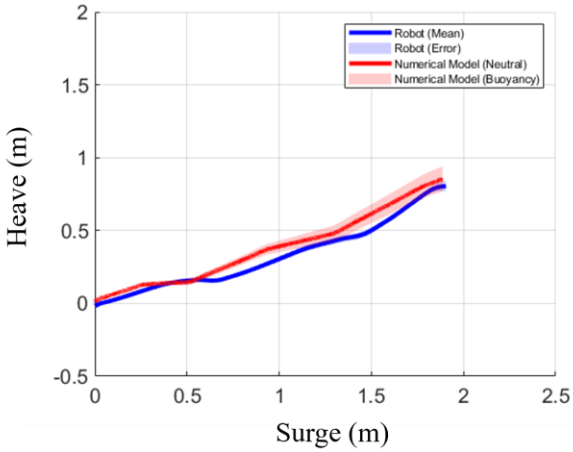

(a)

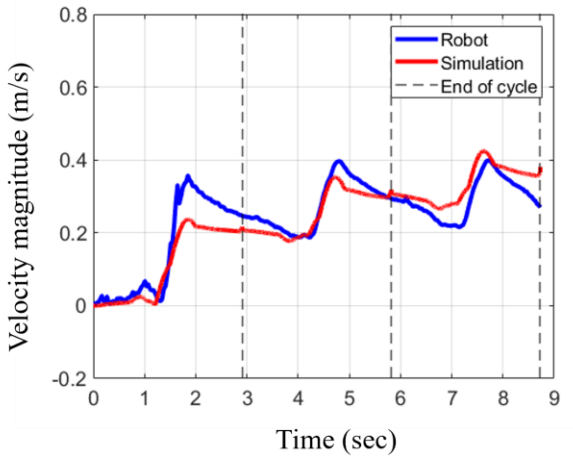

(b)

Figure 3. (a) Position and (b) velocity magnitude when executing the characteristic stroke on the numerical model and the bio-robotic sea lion.

Similarly, in the heave direction, the experimental trials recorded 0.78 m of travel compared to the model's 0.75 m, a difference of 4.0%. The overall root mean squared error (RMSE) between the two center-of-mass trajectories was a low 0.06 m.

A cycle-by-cycle comparison of the mean 2D velocity revealed a progressive increase for both systems, with the numerical model's performance converging with and ultimately surpassing the physical robot. In the first cycle, the numerical model's mean velocity of 0.11 m/s was 27%

TABLE I: MAX. AND MEAN VELOCITY MAGNITUDE FOR EACH CYCLE FOR BIO-ROBOTIC SEA LION AND NUMERICAL MODEL

Velocity Magnitude	**Cycle 1**		**Cycle 2**		**Cycle 3**	
Stroke	Max. ‖V‖ (m/s)	Mean ‖V‖ (m/s)	Max. ‖V‖ (m/s)	Mean ‖V‖ (m/s)	Max. ‖V‖ (m/s)	Mean ‖V‖ (m/s)
CS: Robot	0.36	0.15	0.40	0.27	0.40	0.30
CS: Sim	0.24	0.11	0.35	0.25	0.42	0.33
CS with pelvis: Robot	0.35	0.14	0.38	0.26	0.42	0.31
CS with pelvis: Sim	0.24	0.12	0.36	0.26	0.43	0.35

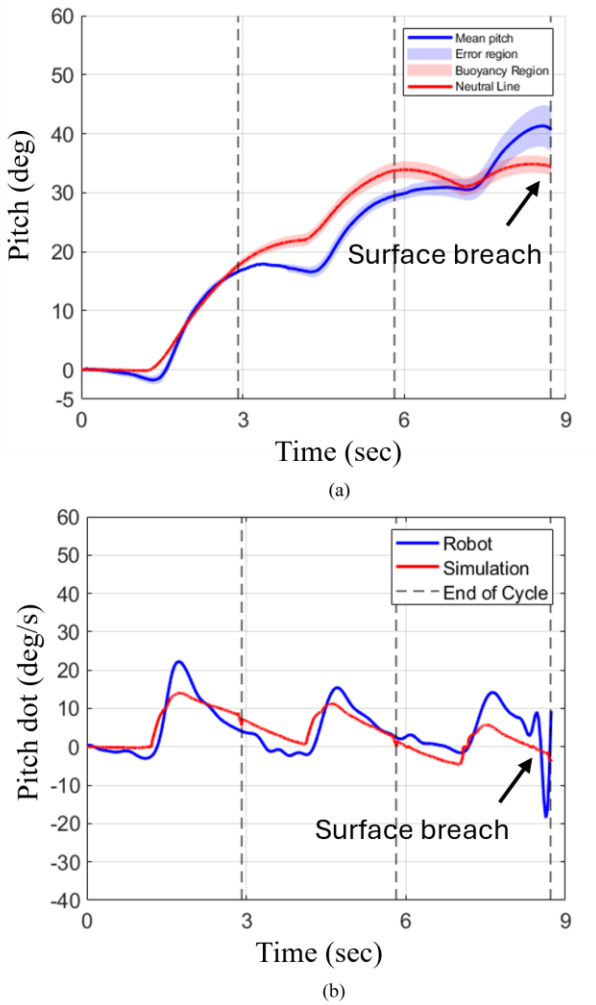

Figure 4. (a) Orientation, and (b) angular rate for bio-robotic sea lion and numerical model during the characteristic stroke.

lower than the experimental result (Fig. 3b, TABLE I). The model's velocity then increased by 36% in the second cycle to 0.15 m/s, narrowing the performance gap to just 7% below the physical robot. In the final cycle, a further 32% increase brought the model's mean velocity to 0.25 m/s, outperforming the experimental system by 10%.

The maximum magnitude of 2d velocity of the numerical model increased consistently across each stroke cycle, whereas the robotic system showed an increase from cycle 1 to cycle 2, but remained constant in cycle 3 (TABLE I). In the first cycle, the model's maximum velocity was 0.24 m/s, or 33% lower than the robot's peak velocity. By the second cycle, the model's velocity increased by 46% to 0.35m/s, reducing the performance gap to 14% below the robot. In the final cycle, the model's velocity continued to increase by another 20% to 0.42m/s, ultimately surpassing the robot's plateaued performance by 5%.

Both systems exhibited a progressive increase in final pitch angle over the three cycles, with the numerical model aligning most closely with the experimental results during the second cycle (Fig. 4a, TABLE II). At the end of the first cycle, the model's final pitch of 12.02° was 29% lower than the 16.89° recorded for the physical robot. The two systems then converged in the second cycle, where the model's 30.65° pitch closely matched the robot's 29.43°. This alignment diverged again in the final cycle, as the model's 35.15° pitch ended up 17% lower than the robot's 42.16°. The overall root mean squared error (RMSE) for the entire pitch trajectory was 6.4°.

The maximum angular velocity was highest during cycle 1 for both the numerical model and the bio-robotic sea lion, followed by a decline in subsequent cycles (Fig. 4b, TABLE II). In the first cycle, the model's peak angular velocity of 10.93°/s was 52% lower than the robot's 22.62°/s. By the second cycle, the model's peak dropped to 8.95°/s, narrowing the gap to 40% below the robot's 14.85°/s. In the final cycle, the trends diverged: the model's velocity fell sharply again to 4.35°/s, while the robot's slightly increased, resulting in the model underperforming by approximately 71%.

In contrast to other metrics, the mean angular velocity showed opposing trends between the two systems (TABLE I). The numerical model's mean velocity first increased by 32%, from 4.68°/s in cycle 1 to 6.17°/s in cycle 2, before dropping sharply in cycle 3. Conversely, the bio-robotic sea lion's velocity followed the opposite pattern, decreasing from cycle 1 to 2 before increasing again in cycle 3.

B. Characteristic Stroke with Pelvis Actuation

The numerical model closely aligned with the bio-robotic sea lion when the characteristic stroke was implemented with pelvis. When comparing the trajectories of both systems, the RMSE was 0.04m. For example, for the bio robotic system, the total translation in surge was 2.01m (Fig.

TABLE II: ANGULAR POSITION AND VELOCITY FOR EACH CYCLE FOR BIO-ROBOTIC SEA LION AND NUMERICAL MODEL

Orientation	**Cycle 1**			**Cycle 2**			**Cycle 3**		
Stroke	Final θ (deg)	Max. θ dot (deg/sec)	Mean θ dot (deg/sec)	Final θ (deg)	Max. θ dot (deg/sec)	Mean θ dot (deg/sec)	Final θ (deg)	Max. θ dot (deg/sec)	Mean θ dot (deg/sec)
CS: Robot	16.89	22.62	5.81	29.43	14.85	4.31	42.16	15.16	4.82
CS: Sim	12.02	10.93	4.68	30.65	8.95	6.17	35.15	4.35	1.71
CS with pelvis: Robot	8.04	17.56	2.73	5.63	16.72	-0.86	0.94	18.43	-1.61
CS with pelvis: Sim	1.58	24.39	0.81	3.15	21.77	0.87	-1.88	23.73	-1.37

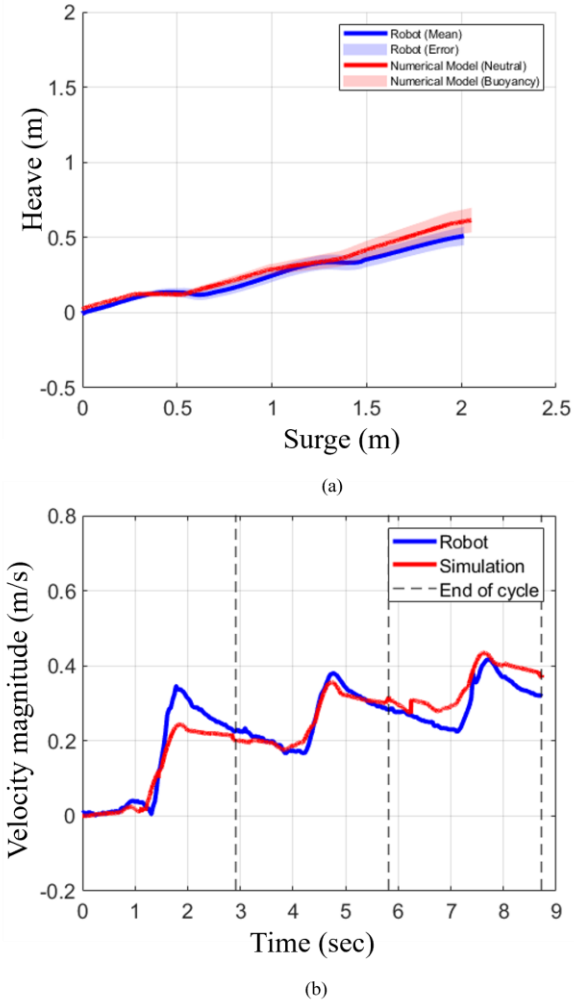

Figure 5. (a) Position and (b) velocity magnitude when executing the characteristic stroke with pelvis actuation.

5a). The numerical model translated a total of 2.05m, which was only 2% higher. Similarly, when the same stroke was executed on the bio robotic system, total translation in heave was 0.51m. In the numerical model, the total translation was 0.61m which was about 20% higher.

The maximum magnitude of 2d velocity for the numerical model and the bio-robotic platform closely matched during cycles 2 and 3, with a slight deviation observed in cycle 1 where the model predicted a lower value (Fig. 5b, TABLE I). In the first cycle, the model's peak velocity of 0.24 m/s was 31% lower than the experimental result. By the second cycle, the model's peak increased to 0.36 m/s, reducing the difference to just 5% below the robot. In the final cycle, the model reached a peak velocity of 0.43 m/s, outperforming the physical robot by 2%.

Both systems showed a consistent, progressive increase in mean 2D velocity across all three cycles, with the strongest alignment occurring in the second cycle. In the first cycle, the numerical model's mean velocity was 16% lower than the 0.14 m/s achieved by the physical robot (TABLE I). By the second cycle, the systems converged, with both achieving an identical mean velocity of 0.26 m/s. In the final cycle, the model's performance was 13% lower than the robot's mean velocity of 0.35 m/s.

The final pitch angle showed a similar trend for both systems, resulting in a low overall trajectory RMSE of 3.3°. At the end of the first cycle, the numerical model's final pitch was 38% lower than the 8.44° recorded by the physical robot (Fig. 6a, TABLE II). The systems then converged in the second cycle, exhibiting nearly identical final pitch angles. By the final cycle, a gap re-emerged, with the model's pitch ending up 34% lower than the robot's 14.45°.

Both systems followed a similar trend for maximum angular velocity, peaking in the second cycle before declining, though the numerical model consistently produced lower values. In the first cycle, the model's peak of 9.01°/s was approximately 43% lower than the robot's 15.67°/s (Fig. 6b, TABLE II). Both systems peaked in the second cycle, where the model's 13.07°/s was about 36% lower than the robot's 20.31°/s. In the final cycle, both velocities decreased,

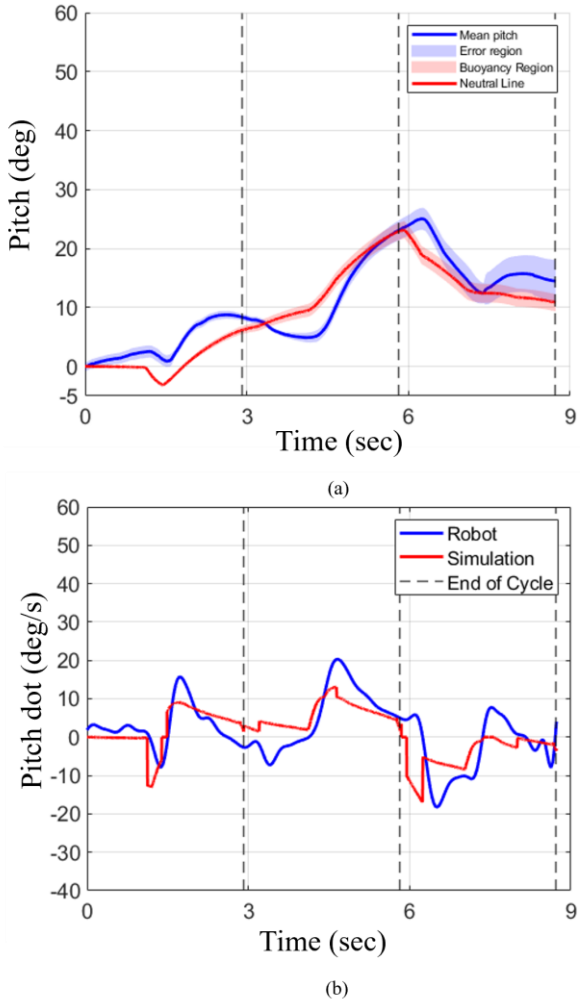

Figure 6. (a) Orientation and (b) angular rate for bio-robotic sea lion and numerical model during the characteristic stroke with pelvis actuation.

with the model's 3.53°/s being roughly 65% lower than the robot's 9.94°/s.

The mean angular velocity for both systems followed similar trends, with closely aligned values in the first two cycles and a larger deviation in the third. In the first cycle, the numerical model's mean angular velocity was 35% lower than the 2.86°/s recorded for the robot (TABLE II). The gap narrowed in the second cycle, where the model's performance was just 14% lower than the robot's mean velocity of 5.07°/s. However, the deviation increased significantly in the final cycle, with the model's mean velocity ending up 47% lower than the robots.

C. Pitch and Yaw Maneuvers

The numerical model accurately predicted performance during maneuvering trials that involved simultaneous head and pelvis actuation, showing strong alignment with the experimental data for both pitch and yaw (Fig. 7). For the pitch maneuver (Fig. 7a), the model's final orientation of 55.46° was only 6% lower than the physical robot, and its mean angular position was 10% lower. The overall trajectory comparison for this maneuver yielded a RMSE of 5.23°. Similarly, for the yaw maneuver, the predicted final orientation of 24.23° was just 8% lower than the experimental result, though its mean angular position was 6% higher. The yaw trajectory (Fig. 7b) showed an even closer match, with a final RMSE of only 1.62°.

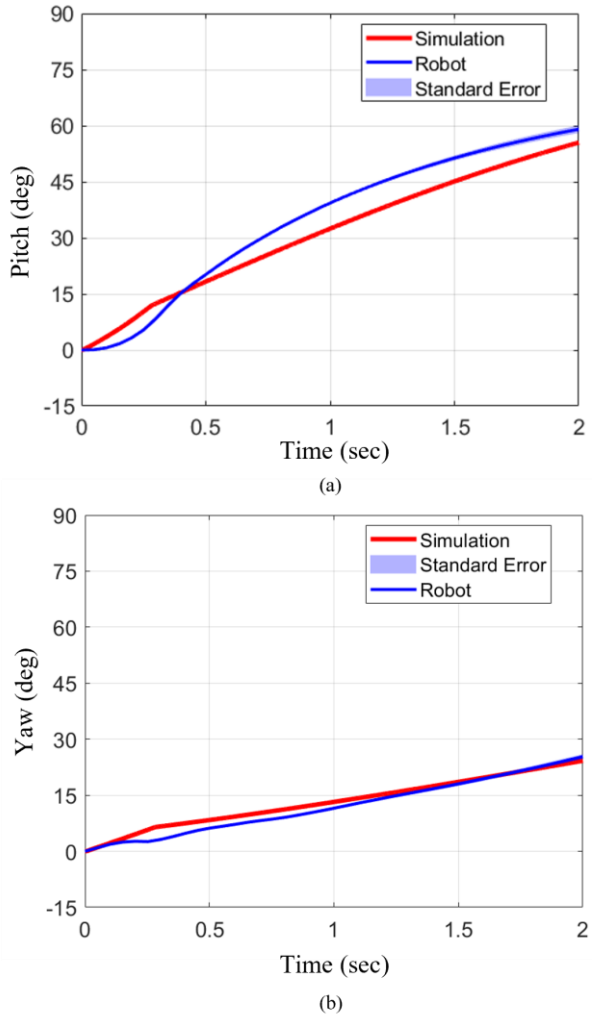

Figure 7. Orientation of the bio-robotic sea lion and the numerical model when head and pelvis were simultaneously actuated to 60° during (a) pitch, and (b) yaw maneuvers.

IV. DISCUSSION

This study successfully developed and validated a numerical model of a bio-robotic sea lion, demonstrating strong agreement between simulation and experiment, particularly for surge and rotational maneuvers. Deviations were most notable in the heave direction, which are likely attributable to unmodeled complexities such as buoyancy changes, body-fluid interactions and the dynamics of water ingress within the robot's open-body structure. During the characteristic stroke, near the end of cycle 3, the pitch data showed a larger deviation between the experimental trials and the numerical model, likely due to the robot breaching the water surface.

A key challenge was the initial underestimation of hydrodynamic coefficients derived from standard computational methods like CFD and strip theory. This discrepancy likely stemmed from several sources: unmodeled buoyancy changes, internal water movement, and a simplifying geometric assumption that treated the robot's body as a prolate spheroid. To overcome this, a GA was employed to systematically refine these coefficients, which significantly improved the model's alignment with the experimental data.

While the optimized hydrodynamic coefficients demonstrated good predictive capability across multiple stroke types and maneuvering trials, a formal parametric sensitivity study over a broader range of stroke amplitudes and frequencies was not conducted. Future work will examine whether the optimized hydrodynamic coefficients accurately represent the dynamics of the system under a wider variety of stroke frequencies, amplitudes, and maneuvering conditions.

Future work should focus on two key areas. First, a direct comparison of joint torques between the model, and the robot is needed to validate the model's prediction of underlying fluid forces, not just the resulting motion. Second, more comprehensive experiments that quantify buoyancy changes and internal water dynamics would enable further refinement of the hydrodynamic coefficients and enhance the model's overall fidelity. Dedicated buoyancy characterization experiments should be conducted prior to swimming trials to reduce uncertainty in hydrostatic parameters. The robot could be statically submerged and evaluated for neutral buoyancy and horizontal trim before actuation to ensure consistency with model assumptions. In addition, water ingress effects in the robot can be experimentally quantified and compared with values

estimated from GA. Towing experiments using a carriage with encoder-based force measurements under prescribed acceleration profiles would enable direct comparison between measured forces and theoretical predictions, providing validation of the optimized hydrodynamic coefficients. Furthermore, incorporating unsteady flow phenomena such as vortex shedding and wake interactions between body segments into the numerical framework may improve its fidelity.

Ultimately, the validated numerical model developed in this study serves as a powerful tool for future research. It enables rapid, large-scale parametric studies to optimize swimming gaits and control strategies, significantly reducing the need for extensive physical prototyping. Furthermore, the model provides an ideal training environment for reinforcement learning, allowing for safe and efficient development of autonomous endeavors.

V. Conclusion

This study successfully developed and validated a high-fidelity numerical model of a bio-robotic sea lion, demonstrating strong agreement with experimental data across various swimming and maneuvering trials. A key contribution of this work is the demonstration that a GA can effectively refine hydrodynamic coefficients, overcoming the inherent limitations of conventional analytical and computational methods. This hybrid methodology provides a more accessible and efficient pathway for developing accurate models of other complex, multi-body underwater robots, thereby advancing the design and control of future bio-inspired autonomous systems.

Acknowledgment

The authors would like to thank all members of the Laboratory for Biological Systems Analysis for their help with reviewing the manuscript. The authors would also like to thank Megan Leftwich and Frank Fish for countless sea lion videos and biological insight. The authors would also like to thank undergraduate students who helped with experimentation and data collection: Anthony Paul Bibeck and Ahmet Yalim Kiral.

References

[1] B. Sun *et al.*, "Recent Progress in Modeling and Control of Bio-Inspired Fish Robots," *Journal of Marine Science and Engineering*, vol. 10, no. 6, Art. no. 6, Jun. 2022, doi: 10.3390/jmse10060773.

[2] G. Li, G. Liu, D. Leng, X. Fang, G. Li, and W. Wang, "Underwater Undulating Propulsion Biomimetic Robots: A Review," *Biomimetics*, vol. 8, no. 3, Art. no. 3, Jul. 2023, doi: 10.3390/biomimetics8030318.

[3] F. E. Fish, "Advantages of aquatic animals as models for bio-inspired drones over present AUV technology," *Bioinspir. Biomim.*, vol. 15, no. 2, p. 025001, Feb. 2020, doi: 10.1088/1748-3190/ab5a34.

[4] A. P. Mignano, S. Kadapa, A. C. Drago, G. V. Lauder, H. G. Kwatny, and J. L. Tangorra, "Fish robotics: multi-fin propulsion and the coupling of fin phase, spacing, and compliance," *Bioinspir. Biomim.*, vol. 19, no. 2, p. 026006, Jan. 2024, doi: 10.1088/1748-3190/ad1dba.

[5] A. P. Mignano, S. Kadapa, J. L. Tangorra, and G. V. Lauder, "Passing the Wake: Using Multiple Fins to Shape Forces for Swimming," *Biomimetics*, vol. 4, no. 1, Art. no. 1, Mar. 2019, doi: 10.3390/biomimetics4010023.

[6] R. Baines *et al.*, "Multi-environment robotic transitions through adaptive morphogenesis," *Nature*, vol. 610, no. 7931, pp. 283–289, Oct. 2022, doi: 10.1038/s41586-022-05188-w.

[7] "Soft-robotic green sea turtle (Chelonia mydas) developed to replace animal experimentation provides new insight into their propulsive strategies | Scientific Reports." Accessed: Feb. 25, 2025. [Online]. Available: https://www.nature.com/articles/s41598-023-37904-5

[8] T. S. Vaquero, G. Daddi, and + 46 Authors, "EELS: Autonomous snake-like robot with task and motion planning capabilities for ice world exploration | Science Robotics." Accessed: Feb. 25, 2025. [Online]. Available: https://www.science.org/doi/10.1126/scirobotics.adh8332

[9] E. Kelasidi, P. Liljeback, K. Y. Pettersen, and J. T. Gravdahl, "Innovation in Underwater Robots: Biologically Inspired Swimming Snake Robots," *IEEE Robotics & Automation Magazine*, vol. 23, no. 1, pp. 44–62, Mar. 2016, doi: 10.1109/MRA.2015.2506121.

[10] A. A. Transeth, R. I. Leine, C. Glocker, K. Y. Pettersen, and P. Liljeback, "Snake Robot Obstacle-Aided Locomotion: Modeling, Simulations, and Experiments," *Trans. Rob.*, vol. 24, no. 1, pp. 88–104, Feb. 2008, doi: 10.1109/TRO.2007.914849.

[11] G. Go and H. T. Ahn, "Hydrodynamic derivative determination based on CFD and motion simulation for a tow-fish," *Applied Ocean Research*, vol. 82, pp. 191–209, Jan. 2019, doi: 10.1016/j.apor.2018.10.023.

[12] "Mathematical Biofluiddynamics | SIAM Publications Library," CBMS-NSF Regional Conference Series in Applied Mathematics. Accessed: Feb. 18, 2026. [Online]. Available: https://epubs.siam.org/doi/book/10.1137/1.9781611970517

[13] D. Hopkin, M. Davies, and I. Gartshore, "The aerodynamics and control of a remotely-piloted underwater towed vehicle," *Canadian Aeronautics and Space Journal*, 1990, Accessed: Feb. 26, 2025. [Online]. Available: https://www.semanticscholar.org/paper/The-aerodynamics-and-control-of-a-remotely-piloted-Hopkin-Davies/6fdec78d87298bb7fa559ae2c8e35d4afe59251c

[14] M. Moonesun, M. Javadi, P. Charmdooz, Karol, and U. Mikhailovich, "Evaluation of submarine model test in towing tank and comparison with CFD and experimental formulas for fully submerged resistance," *Indian Journal of Geo-Marine Sciences*, vol. 42, pp. 1049–1056, Dec. 2013.

[15] W. Wang and C. M. Clark, "Modeling and Simulation of the VideoRay Pro III Underwater Vehicle," in *OCEANS 2006 - Asia Pacific*, May 2006, pp. 1–7. doi: 10.1109/OCEANSAP.2006.4393862.

[16] C. Wang, F. Zhang, and D. Schaefer, "Dynamic modeling of an autonomous underwater vehicle," *Journal of Marine Science and Technology*, vol. 20, pp. 199–212, Aug. 2015, doi: 10.1007/s00773-014-0259-0.

[17] G. a. C. T. Bandara, D. a. a. C. Ratnaweera, and D. H. S. Maithripala, "Modeling and Control Approach for a Complex-Shaped Underwater Vehicle," *American Journal of Mechanical Engineering*, vol. 7, no. 4, Art. no. 4, Oct. 2019, doi: 10.12691/ajme-7-4-2.

[18] M. Nahon, "A simplified dynamics model for autonomous underwater vehicles," in *Proceedings of Symposium on Autonomous Underwater Vehicle Technology*, Jun. 1996, pp. 373–379. doi: 10.1109/AUV.1996.532437.

[19] A. Drago, S. Kadapa, N. Marcouiller, H. G. Kwatny, and J. L. Tangorra, "Using Reinforcement Learning to Develop a Novel Gait for a Bio-Robotic California Sea Lion," *Biomimetics*, vol. 9, no. 9, Art. no. 9, Sep. 2024, doi: 10.3390/biomimetics9090522.

[20] N. Marcouiller *et al.*, "Development of a Bio-robotic Swimmer Based on the California Sea Lion," Sep. 11, 2025, *Research Square*. doi: 10.21203/rs.3.rs-7455024/v1.

[21] F. S. Malvestuto and L. J. Gale, "Formulas for additional mass corrections to the moments of inertia of airplanes." Feb. 01, 1947. Accessed: Feb. 26, 2025. [Online]. Available: https://ntrs.nasa.gov/citations/19930082122

[22] J. Legriel, C. Le Guernic, S. Cotton, and O. Maler, "Approximating the Pareto Front of Multi-criteria Optimization Problems," in *Tools and Algorithms for the Construction and Analysis of Systems*, J. Esparza and R. Majumdar, Eds., Berlin, Heidelberg: Springer, 2010, pp. 69–83. doi: 10.1007/978-3-642-12002-2_6.